Biochimica et Biophysica Acta 1840 (2014) 2050–2059

Contents lists available at ScienceDirect

Biochimica et Biophysica Acta

journal homepage: www.elsevier.com/locate/bbagen

G-quadruplex DNA recognition by nucleophosmin: New insights from protein dissection

Pasqualina Liana Scognamiglio [a,c,1], Concetta Di Natale [a,c,1], Marilisa Leone [d,b], Mattia Poletto [e], Luigi Vitagliano [d], Gianluca Tell [e], Daniela Marasco [a,b,*]

[a] Department of Pharmacy, University of Naples "Federico II", DFM-Scarl, 80134 Naples, Italy
[b] CIRPEB: Centro Interuniversitario di Ricerca sui Peptidi Bioattivi, University of Naples "Federico II", DFM-Scarl, 80134 Naples, Italy
[c] Center for Advanced Biomaterials for Healthcare@CRIB, Istituto Italiano di Tecnologia (IIT), 80125 Naples, Italy
[d] Institute of Biostructures and Bioimaging, CNR, 80134 Naples, Italy
[e] Department of Medical and Biological Sciences, University of Udine, 33100 Udine, Italy

ARTICLE INFO

Article history:
Received 16 December 2013
Received in revised form 13 February 2014
Accepted 18 February 2014
Available online 24 February 2014

Keywords:
Disordered protein region
Surface Plasmon Resonance
Helical stability

ABSTRACT

Background: Nucleophosmin (NPM1, B23) is a multifunctional protein that is involved in a variety of fundamental biological processes. NPM1/B23 deregulation is implicated in the pathogenesis of several human malignancies. This protein exerts its functions through the interaction with a multiplicity of biological partners. Very recently it is has been shown that NPM1/B23 specifically recognizes DNA G-quadruplexes through its C-terminal region.
Methods: Through a rational dissection approach of protein here we show that the intrinsically unfolded regions of NPM1/B23 significantly contribute to the binding of c-MYC G-quadruplex motif. Interestingly, the analysis of the ability of distinct NPM1/B23 fragments to bind this quadruplex led to the identifications of distinct NPM1/B23-based peptides that individually present a high affinity for this motif.
Results: These results suggest that the tight binding of NPM1/B23 to the G-quadruplex is achieved through the cooperation of both folded and unfolded regions that are individually able to bind it. The dissection of NPM1/B23 also unveils that its H1 helix is intrinsically endowed with an unusual thermal stability.
Conclusions: These findings have implications for the unfolding mechanism of NPM1/B23, for the G-quadruplex affinity of the different NPM1/B23 isoforms and for the design of peptide-based molecules able to interact with this DNA motif.
General observation: This study sheds new light in the molecular mechanism of the complex NPM1/G-quadruplex involved in acute myeloid leukemia (AML) disease.

1. Introduction

Nucleophosmin (NPM1, also known as B23, No38 and numatrin) is an abundant multifunctional protein, initially identified as a phosphoprotein, which is present in high quantities in the granular region of nucleoli [1,2]. NPM1/B23 is, however, capable of shuttling between nucleus and cytoplasm [3]. NPM1/B23 plays a plethora of functions including the regulation of ribosome biogenesis, chromatin remodeling, DNA replication, recombination, transcription, repair and the control of centrosome duplication [4,5]. This protein has been found over-expressed in tumors of different histological origins, including gastric, ovarian, bladder and prostate carcinomas and in various hematological malignancies [6–9]. Notably, NPM1/B23 has been identified as the most frequently mutated gene in acute myeloid leukemia (AML) patients, accounting for approximately 30% of cases [10–14].

NPM1/B23 belongs to the nucleophosmin/nucleoplasmin family of proteins [15]. Three distinct isoforms of the protein have been reported to be expressed in human cells. B23.1, the longest and the most abundant, is also the best characterized isoform. B23.2 and B23.3 are splicing

Abbreviations: TIS, Triisopropylsilane; TFA, Trifluoroacetic acid; DMF, Dimethylformamide; DCM, Dichloromethane; HBTU, 1-H-Benzotriazolium, 1-[bis(dimethylamino)methylene]-hexafluorophosphate(1-), 3 oxide; HOBt, N-hydroxybenzotriazole; DIEA, Di-isopropylethylamine; Fmoc, Fluorenylmethoxycarbonyl; TCEP, Tris(2-Carboxyethyl) phosphine; HPLC, High Performance Liquid Chromatography; LC–MS, Liquid Chromatography–Mass Spectrometry; EDC, 1-Ethyl-3-[3-dimethylaminopropyl]carbodiimide hydrochloride; NHS, N-hydroxysuccinimide; NOESY, Nuclear Overhauser Enhancement Spectroscopy; RMSD, Root Mean Square Deviation; TOCSY, Total Correlation Spectroscopy; C_53 NPM1, NPM1 242–294; C_70 NPM1, NPM1 225–294; C_107 NPM1, NPM1 188–294

* Corresponding author at: Department of Pharmacy, University "Federico II", Via Mezzocannone, 16, 80134 Naples, Italy. Tel.: +39 081 2532043; fax: +39 081 2534574.
E-mail address: daniela.marasco@unina.it (D. Marasco).

[1] These are co-first authors.

http://dx.doi.org/10.1016/j.bbagen.2014.02.017
0304-4165/

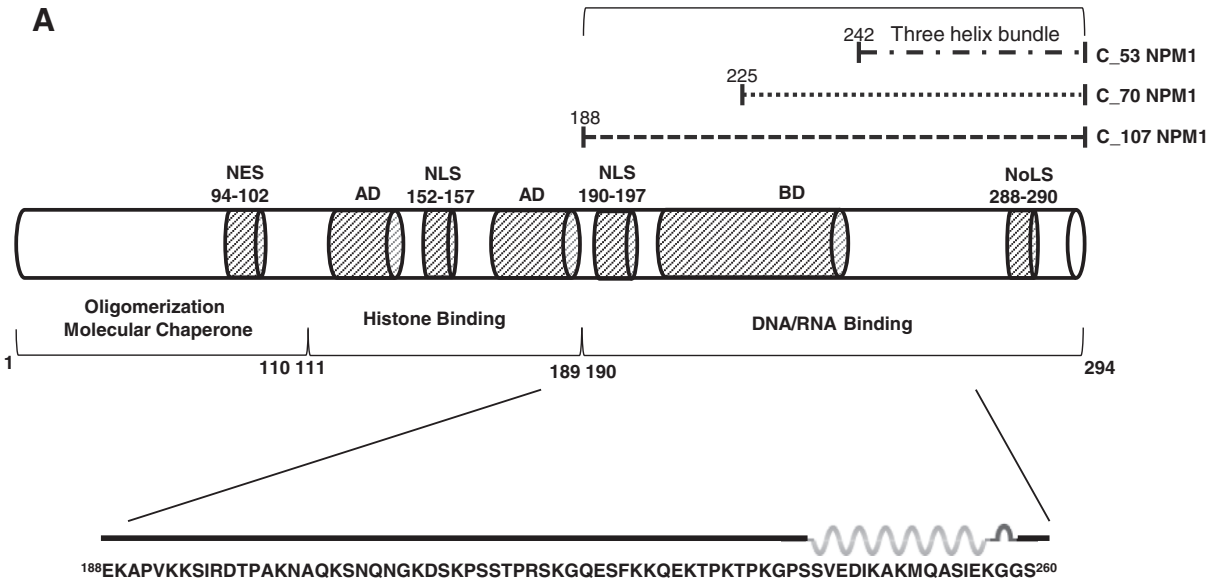

B

188-225	EKAPVKKSIRDTPAKNAQKSNQNGKDSKPSSTPRSKGQ
225-243	QESFKKQEKTPKTPKGPSS
242-259 B23.1	SSVEDIKAKMQASIEKGG
242-259 B23.2	SSVEDIKAKMQASIEKAH
259-277 B23.1	GSLPKVEAKFINYVKNCFR

Fig. 1. Schematic representation of NPM1 protein. (A) The modular structure of NPM1, functional, structural domains and primary structure of C_107NPM1 are pointed out and (B) primary sequences of C_107NPM1-based peptides were analyzed in this study.

variants that lack the C-terminal 35 amino-acids and a 29 amino-acid stretch (residues 195–223) in the basic region, respectively [16].

Structural characterizations of B23.1 have shown that the protein is endowed with a modular structure (Fig. 1). The N-terminal domain extends for approximately 100 residues and displays an eight-stranded beta-barrel fold. Five N-terminal domains oligomerize to form a crown-shaped pentamer [17]. Two or more of these pentamers may associate to form decamers or higher oligomeric species [18]. The central portion of NPM1 is characterized by the presence of two acid domains (residues 119–133 and 161–188) and a basic region (residues 198–239). The C-terminal domain (CTD) of B23.1 forms a globular structure consisting of a three helix bundle. The destabilization of this structural unit abolishes the nucleolar localization of the protein [19]. The C-terminal region of the protein has also been the subject of a number of intriguing investigations aimed at unveiling its folding mechanism [20–23]. Despite the structural heterogeneity of the different regions of the protein, recent biophysical studies have highlighted their mutual stabilization upon treatments with temperature or chemical denaturants [21,24].

The analysis of the NPM1/B23 sequence also shows that the protein shuttling abilities between intracellular compartments rely on several signaling sequences: i) a NES (nuclear export) motif with two leucines in the N-terminal domain, ii) NLSs (nuclear localization) between the two acidic stretches and, iii) a NoLS (nucleolar localization) with aromatic-rich residues at the C-terminal domain [20]. NPM1/B23 exerts its functions essentially through interactions with a variety of biological partners. NPM1 interactions with other proteins (e.g. p53, p14arf, Fbw7γ, APE-1) [25–29], ribosomal proteins RPL5, RPS9, RPL23, HIV proteins REV TAT) [30] are generally mediated by the N-terminal domain, whereas the C-terminal moiety regulates the binding of DNA/RNA.

NPM1 was shown to bind both DNA and RNA oligonucleotides, with a preference for single stranded structures with respect to those double-stranded, independently of the sequence [31,32].

Recently, it is has been shown that the C-terminus of NPM1 is able to specifically recognize G-quadruplex DNA motifs [33,34]. This finding is of great interest since these motifs are attractive targets for tumor treatment for their selective localization on promoters of several oncogenes and on telomeric regions [34,35]. In particular, it has been demonstrated that the NPM1 C-terminal domain recognizes in vitro a well-characterized G-quadruplex forming sequence present at the NHEIII region of the c-MYC oncogene promoter [33]. This promoter region adopts a G-quadruplex structure both in vitro and in vivo, regulating up to 90% of the total c-MYC transcriptional rate [36]. NMR studies have shown that this G-quadruplex is recognized by NPM1 primarily by residues belonging to the helices H1 and H2 of the three-helix bundle. Nevertheless, mutagenesis analyses have shown that a fundamental contribution to the G-quadruplex binding is provided by the residues Lys 229 and Lys 230 [34]. Intriguingly, the region embedding these residues is disordered in the NMR structure of the complex. Attempts to explain these puzzling findings were based on the observation that the presence of an unstructured segment adjacent to the interacting domain could provide a larger platform for long-range electrostatic interactions or transient physical contacts [34].

In order to gain further insights into this intricate recognition mechanism, here we evaluated the ability of individual fragments of NPM1 to bind this G-quadruplex. Interestingly, the dissection of NPM1 led to the identification of distinct protein segments that present high affinity for this motif. The structural characterization of these fragments provides new clues about the folding/unfolding process of the triple helix bundle

motif. Moreover, present findings delineate strategies for the development of peptide-based entities for targeting the c-MYC G-quadruplex.

2. Material and methods

2.1. Preparation of recombinant C_107 NPM1

C_107 NPM1 (residues 188–294) constructs were expressed and purified as HisTag-fusion proteins in *Escherichia coli* BL21 (DE3) following or adapting the procedure previously described [37]. The quality of purification was checked by Coomassie-stained SDS-polyacrylamide gel electrophoresis (PAGE) analysis. Extensive dialysis against PBS was performed to remove any trace of imidazole from the purified proteins.

2.2. G-quadruplex

Oligonucleotide TGGGGAGGGTGGGGAGGGTGGGGAAGG biotinylated at the 5′-end used in this study was purchased from PRIMM s.r.l (Milan, Italy) and purified by HPLC. For annealing, as already reported, in 20 mM Hepes, pH 7.0, with 100 mM NaCl, oligo was heated to 95 °C for 15 min and slowly cooled down at RT, overnight.

2.3. Surface Plasmon Resonance

The interactions between biotinylated c-MYC G-quadruplex with purified C_107 NPM1, and peptides NPM1 188–225, 225–243, 242–259 and 242–259_B23.2, were all measured using the SPR technique and BIAcore T-100, 3000 (GE Healthcare Milano, Italy). Biotinylated c-MYC G-quadruplex was immobilized on a sensor chip SA, pre-coated with streptavidin (GE Healthcare Milano, Italy). The capturing procedure on the biosensor surface was performed as reported in [38]. Running buffer was Hepes-buffered saline-EP, which contains 10 mM Hepes, pH 7.4, 0.15 M NaCl, 3 mM EDTA, 0.005% (v/v) surfactant P20. Analytes were dissolved in running buffer, and binding experiments were performed at 25 °C with a flow rate of 20 μL/min. The association phase (k_{on}) was followed for 180 s, whereas the dissociation phase (k_{off}) was followed for 300 s. The complete dissociation of active complex formed was achieved by addition of 1 M NaCl, for 60 s before each new cycle start. The reference chip sensorgrams were opportunely subtracted to sample sensorgrams. When experimental data met quality criteria, kinetic parameters were estimated assuming a 1:1 binding model and using version 4.1 Evaluation Software (GE Healthcare), and it was so only for C_107 NPM1. Conversely, for C_107 NPM1 derived peptides the fit of the equilibrium values for the SPR response vs. the ligand concentration was employed and performed with GraphPad Prism v4.00 [39] using the one-site binding equation.

2.4. Peptide synthesis

Reagents for peptide synthesis (Fmoc-protected amino acids and resins, activation and deprotection reagents) were from Novabiochem (Läufelfingen, Switzerland) and InBios (Napoli, Italy). Solvents for peptide synthesis and HPLC analyses were from Romil (Dublin, Ireland); reversed phase columns for peptide analysis and the LC–MS system were from ThermoFisher (Milan, Italy). Solid phase peptide syntheses were performed on a fully automated multichannel peptide synthesizer Syro I (Multisynthech, Germany). Preparative RP-HPLC was carried out on a Shimadzu LC-8A, equipped with a SPD-M10 AV detector and with a Phenomenex C18 Jupiter column (50 × 22 mm ID; 10 μm). LC–MS analyses were carried out on a LCQ DECA XP Ion Trap mass spectrometer equipped with a OPTON ESI source, operating at 4.2 kV needle voltage and 320 °C with a complete Surveyor HPLC system, comprised of MS pump, an autosampler and a photo diode array (PDA). Narrow bore 50 × 2 mm C18 BioBasic LC–MS columns were used for these analyses.

The peptides 188–225, 225–243, 242–259, 242–259_B23.2, and 259–277 were synthesized employing the solid phase method on a 50 μmol scale following standard Fmoc strategies [40]. Rink-amide resin (substitution 0.5 mmol/g) was used as solid support. Activation of amino acids was achieved using HBTU/HOBt/DIEA (1:1:2), whereas Fmoc deprotection was carried out using a 20% (v/v) piperidine solution in DMF. All couplings were performed for 15 min and deprotections for 10 min and at the end of peptide chain assembly peptides were acetylated at their N-termini. Peptides were removed from the resin by treatment with a TFA:TIS:H2O (90:5:5, v/v/v) mixture for 90 min at room temperature; then crude peptides were precipitated in cold ether, dissolved in a water/acetonitrile (1:1, v/v) mixture and lyophilized.

Products were purified by RP-HPLC applying a linear gradient of 0.1% TFA CH_3CN in 0.1% TFA water from 5% to 65% over 12 min using a semi-preparative 2.2 × 5 cm C18 column at a flow rate of 20 mL/min. Peptides and purity and identity were confirmed by LC–MS. Purified peptides were lyophilized and stored at −20 °C until use.

2.5. Circular dichroism (CD) spectroscopy

CD spectra were recorded on a Jasco J-810 spectropolarimeter (JASCO Corp, Milan, Italy). CD spectra were registered at 25 °C in the far UV region from 190 to 260 nm. Each spectrum was obtained averaging three scans, subtracting contributions from corresponding blanks and converting the signal to mean residue ellipticity in units of $deg*cm^2*dmol^{-1}*res^{-1}$. Other experimental settings were: 20 nm/min scan speed, 2.0 nm band width, 0.2 nm resolution, 50 mdeg sensitivity, and 4 s response. The concentration of peptides was kept at 10×10^{-5} M and a 0.1 cm path-length quartz cuvette was used. Spectra were acquired in 10 mM phosphate buffer at pH 7.0.

Thermal denaturation profiles were obtained by measuring the temperature dependence of the ellipticity at 220 nm in the 293–363 K range with a resolution of 0.5 °C and 1.0 nm bandwidth. The heating rate was 1 K/min and the response at 16 s with a Peltier temperature controller.

A buffer solution containing 10 mM of sodium phosphate was used in chemical denaturation experiments. Urea was purchased from Sigma and further purified by recrystallization from ethanol/water (1:1) mixtures. Stock solutions of urea were mixed with peptide solutions to give a constant final value of the peptide concentration (100 μM). The final concentration of denaturant was in the range 0.0–8.0 M. Each sample was incubated overnight. Longer incubation times led to identical spectroscopic signals.

2.6. NMR experiment

NMR analysis was performed for 242–259 and 242–259_B23.2. NMR samples consisted of peptides (242–259: 1 mg; 242–259_B23.2: 0.8 mg) dissolved in 600 μL of 10 mM sodium phosphate buffer pH = 7.2; samples contained 5% (v/v) D_2O (99.8% d, Armar Scientific, Switzerland). Most NMR spectra were recorded at 298 K on a Varian Unity INOVA 600 MHz spectrometer provided with a cold probe. The process of proton resonance assignment was conducted by following a standard protocol which relies on comparison of 2D[^{1}H, ^{1}H] TOCSY (Total Correlation Spectroscopy) [41] (70 ms mixing time) and NOESY (Nuclear Overhauser Enhancement Spectroscopy) [42] (200 and 300 ms mixing times) spectra. Chemical shifts were referenced with respect to internal TSP (trimethylsilyl-3-propionic acid sodium salt-d4, 99% d, Armar Scientific, Switzerland) (see Appendix Tables A1, A2 for 242–259_B23.1, 242–259_B23.2, respectively).

1D spectra were recorded with a relaxation delay of 1 s and 32–64 scans. 2D experiments were generally acquired with 32–64 scans, 128–256 FIDs in t_1, 1024 or 2048 data points in t_2.

Water suppression was achieved with the DPFGSE (Double Pulsed Field Gradient Selective Echo) [43] sequence. Spectra were processed with VNMRJ 1.1D (Varian by Agilent Technologies, Italy) and analyzed with the NEASY [44] program that is included in the CARA (Computer Aided Resonance Assignment) software package (http://www.nmr.ch/). Analysis of Hα chemical shifts and deviations from random coil values

were estimated with NmrView [45,46] by using the database by Wishart et al. for peptide random coil chemical shift values [47].

For the 242–259 peptide additional NMR spectra (1D [^{1}H] and 2D [^{1}H, ^{1}H] TOCSY (70 ms)) were recorded on a Varian Unity INOVA 400 MHz spectrometer at the following temperatures: 298, 303, 308, 313, 318, 323, and 333 K.

Peptide structure calculations were performed with CYANA [48] (version 2.1). Distance constraints for structure calculations were gained from NOESY experiments (300 ms mixing time). Angular constraints were generated with the GRIDSEARCH module of CYANA. Calculations generally started from 100 random conformers; the 20 structures with the best CYANA target functions (i.e. the lowest values) were inspected with MOLMOL [49].

3. Results

3.1. C_107 NPM1/B23.1 binds c-MYC G-quadruplex with high affinity

Previous investigations have shown that the binding affinity of NPM1 toward the c-MYC G-quadruplex depends on the length of the C-terminal region considered. Indeed, the C_53 NPM1 fragment of the protein (residues 242–294), which exclusively includes the three-helix bundle motif, binds the quadruplex with a K_D of 82 μM. The affinity increases (K_D = 1.9 μM) if an 18-residue stretch of the basic region is added to C_53 to generate C_70 NPM1 (residues 225–294) [33]. Since we have recently shown that the region 188–225 has stabilizing effects on C_70 NPM1, we evaluated the effect of this extension of the C-terminal region on G-quadruplex recognition. In particular, the affinity of C_107 NPM1 (residues 188–294) toward c-MYC G-quadruplex sequence was measured by SPR. A biotinylated oligonucleotide sequence was efficiently immobilized on SA-chip (averaged immobilization level 300 RU) and C_107 NPM1 was employed as analyte (concentration range 0.1–10 μM). Dose–response sensorgrams (Fig. 2) revealed that C_107 NPM1 avidly binds c-MYC G-quadruplex; the association rate appeared to be rapid ($ka = 8.09 * 10^4\ M^{-1}\ s^{-1}$) whereas the dissociation was slow ($kd = 0.0266\ s^{-1}$), thus providing a K_D value of 0.328 μM (Table 1). This finding clearly indicates that C_107 NPM1 presents a higher affinity for the G-quadruplex compared to C_70 and C_53 NPM1. Therefore, in addition to the region 225–241 [33], the region 188–224 also contributes to the complex formation.

3.2. Dissecting the C-terminal region of B23.1 and B23.2

The progressive increase of the affinity for the G-quadruplex upon the addition of extra-fragments on the N-terminal side of the three helix bundle motif, prompted us to dissect the C-terminal region of NPM1 in individual fragments to evaluate their intrinsic structural

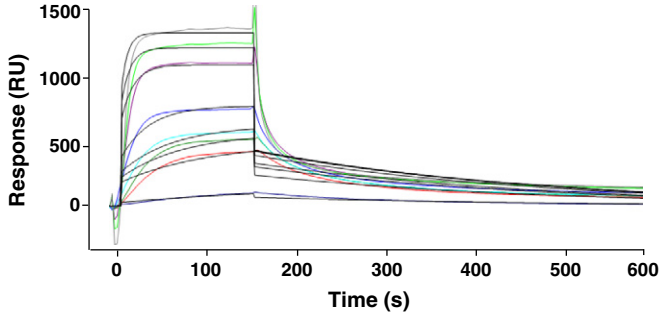

Fig. 2. Binding of C_107 NPM1 with c-MYC G-quadruplex through SPR. Overlay of sensorgrams for the interaction between biotinylated at 5′ c-MYC G-quadruplex sequence immobilized on a SA (streptavidin) sensor chip and C_107 NPM1 (as analyte). Experimental curves (colored lines) related to different concentrations of analyte (0.1, 0.5, 0,8 1, 2, 5, 7, 10 μM) were fitted according to a single exponential binding model with 1:1 stoichiometry (gray lines).

Table 1
Dissociation constants for the interaction of NPM1 regions with c-MYC G-quadruplex.

Ligand	K_D (μM)
C_70 NPM1	1.9 ± 0.1*
C_53 NPM1	82 ± 15*
C_107 NPM1	0.328 ± 0.003
188–225 NPM1	18 ± 5
225–243 NPM1	54 ± 15
242–259 NPM1	275 ± 43

* [33].

preferences and their DNA binding ability. Taking into account present and previous findings, the following fragments of NPM1/B23.1 were considered: 188–225, 225–243 (both belonging to the basic region), 242–259 (Helix 1), and 259–277 (Helix 2). For the region 242–259, a variant corresponding to the C-terminal end of B23.2 (242–259_B23.2) was also investigated (Fig. 1).

3.2.1. Intrinsic structural preferences of fragments of B23.1 and B23.2 C-terminal region

All peptides reported in Fig. 1 were chemically synthesized with good yields by SPPS, using Fmoc methodologies as N-terminal acetylated and C-terminal amidated derivatives and purified by RP-HPLC (see Materials and methods for further details). Their identity and purity (averaged purity > 97%) were assessed by LC–MS (data not shown).

To evaluate the impact of structural preferences of these fragments on their ability to bind c-MYC G-quadruplex, all peptides were characterized by far-UV circular dichroism (CD) and NMR spectroscopies. It is worth mentioning that the intrinsic tendency to aggregate and precipitate of the peptide 259–277 (corresponding to H2) prevented accurate structure and binding analyses.

The CD analysis shows a different structural behavior of the peptides used.

NPM1 188–225 (Fig. 3A) and 225–243 [21] CD spectra show typical random coil profiles presenting only one minimum at around 200 nm, as expected. On the other hand the two variants corresponding to the region 242–259 (242–259_B23.1 and 242–259_B23.2) showed spectra with bands at 190, 205, and 222 nm suggestive of the presence of α-helical conformation (Figs. 3B and A1). This conformation appeared stable within 4 h. Indeed the overlay of CD spectra registered within this time-lapse did not show any variation in the position and intensity of the bands.

In this framework, to gain deeper insights into the structure of the H1 region once separated from protein context, we performed NMR studies on both 242–259 variants.

For 242–259 in phosphate buffer, proton resonance assignments were obtained by comparison of 2D [^{1}H,^{1}H] TOCSY [41] and NOESY experiments [42] (Fig. 4A). Chemical shift deviations from random coil values [47] (Fig. 5a) were then evaluated and indicated a propensity for the peptide to form a helix in the region between Glu245 and Met251 (estimated helical content: 38.9%). The tendency of the peptide to adopt a helical conformation was further verified by NOE pattern [50] (Fig. 4B). Here, several contacts indicative of helices, mainly $H_Ni–H_N(i + 1)$; $H_\alpha i–H_N(i + 2)$; $H_\alpha i–H_N(i + 3)$; and $H_\alpha i–H_\beta(i + 3)$, were observed in the segment encompassing residues Val244–Lys250. However, these NOEs coexist with rather strong sequential contacts of the type $H_\alpha i–H_N(i + 1)$ that are, instead, hallmarks of extended and/or random coil conformations and suggest a certain degree of disorder for the peptide in solution.

To get additional informations, we carried out complete structural calculations. The analysis of the NMR ensemble of structures (Fig. 5B), carried out with the software MOLMOL [49], revealed the presence, in most of the conformers, of a disordered pseudo-helical segment in between Val244 and Met251, composed of a

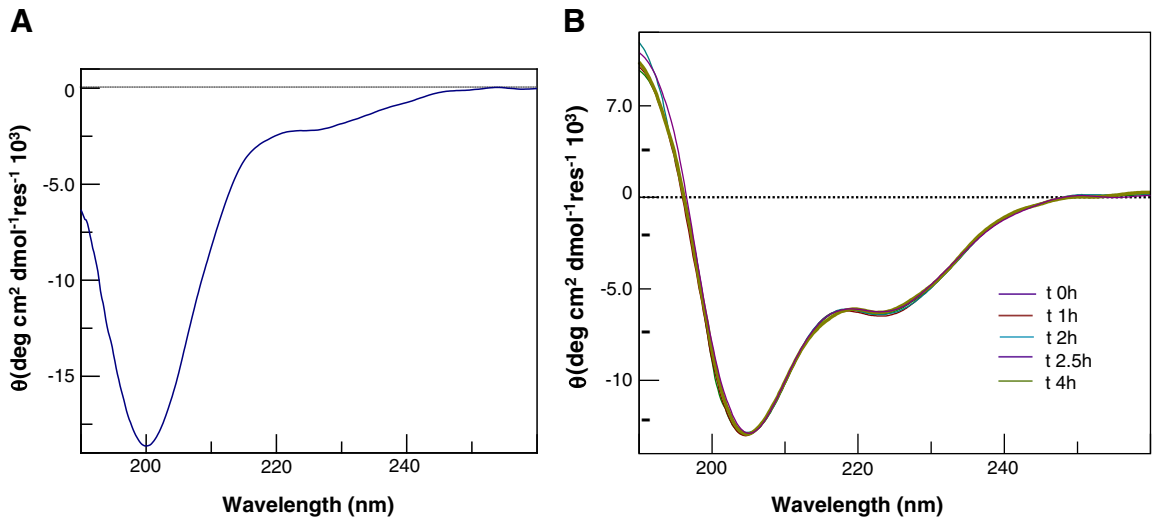

Fig. 3. Circular dichroism studies of C_107NPM1-based peptides. CD spectra of NPM1 (A) 188–225 and (B) 242–259, for the latter the overlay of spectra recorded at different times (0–4 h) is reported, and they were registered at 293 K in 10 mM phosphate buffer, pH 7.2.

turn of 3.10 helix (Val244–Ile247), and of a bend from Ile247 to Met251. This analysis clearly indicates that the C-terminal end is flexible.

NMR conformational analyses were carried out for 242–259_B23.2 in similar experimental conditions. Recorded 2D [^{1}H, ^{1}H] TOCSY and NOESY spectra (Fig. A2) allowed to assign proton resonances also for this peptide. The NMR parameters, i.e. chemical shift deviations from random coil values (Fig. 5g) and NOE pattern (Fig. A3), indicate a similar helix propensity and conformational behavior as 242–259 in the region between Val244 and Ala249. Despite the two amino-acid substitutions occurring at the very end of the two peptides (Fig. 1), the C-terminus of both 242–259 and 242–259_B23.2 is disordered.

3.2.2. The helical fragments 242–259 of B23.1 and B23.2 are endowed with a remarkable stability

The analysis of the thermal and chemical stabilities of 242–259 and 242–259_B23.2 unveils some unexpected features. Spectra collected over the temperature range 293 to 371 K indicate a marginal decrease of the CD signal (Fig. 6A). This experiment indicates that this sequence retains a significant amount of the helical structure at a very high temperature, even if a slight variation of ellipticity at 222 nm in the range 333–371 K (inset of Fig. 6A) suggests that a decrease of total helical content occurs. This thermal stability is very unusual for short peptides and has been occasionally reported for peptides with unnatural constrains [51].

These observations prompted us to perform additional NMR studies to better characterize the influence of higher temperatures on 242–259

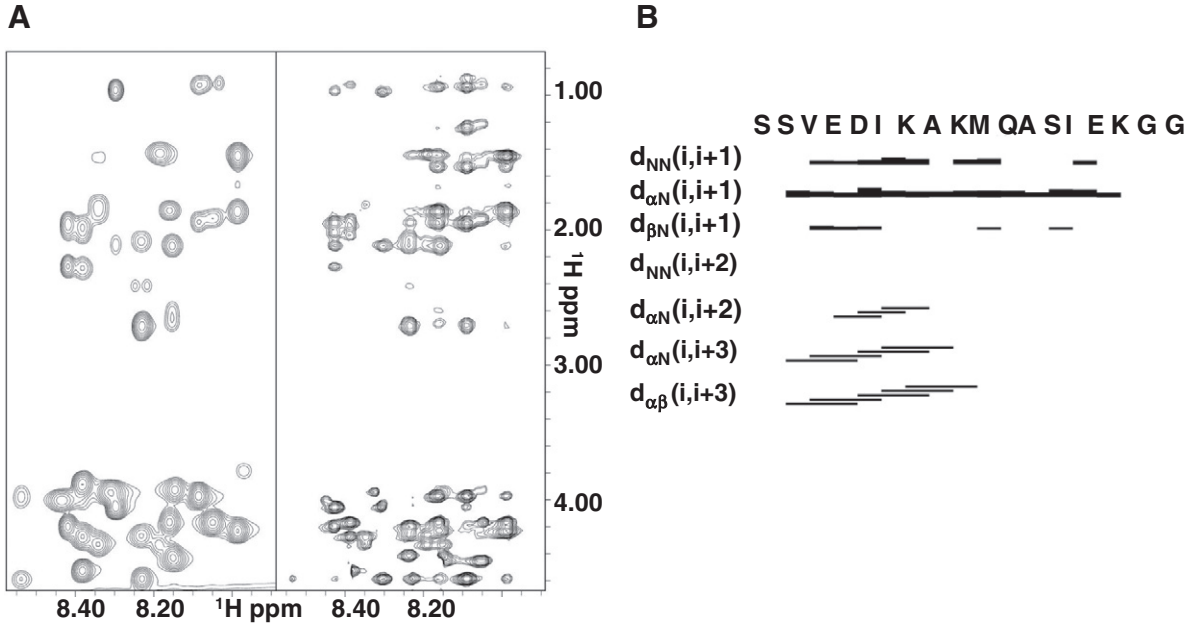

Fig. 4. NMR analysis of NPM1 242–259 B23.1 peptide. (A) 2D [^{1}H, ^{1}H] TOCSY (70 ms mixing time) (left panel) and 2D [^{1}H, ^{1}H] NOESY (300 ms mixing time) (right panel), the HN-aliphatic proton correlation region is shown. (B) NOE intensity diagrams for NPM1 242–259 B23.1. The amino acid sequence is reported on the top of diagram with the one letter code. A NOE connectivity between the Hx and Hy protons in the i and i + z residue respectively is indicated with "*d*xy(i, i + z)". The thickness of the bars reflects the corresponding NOE intensity. The software CYANA [48] was used to generate the NOE diagram.

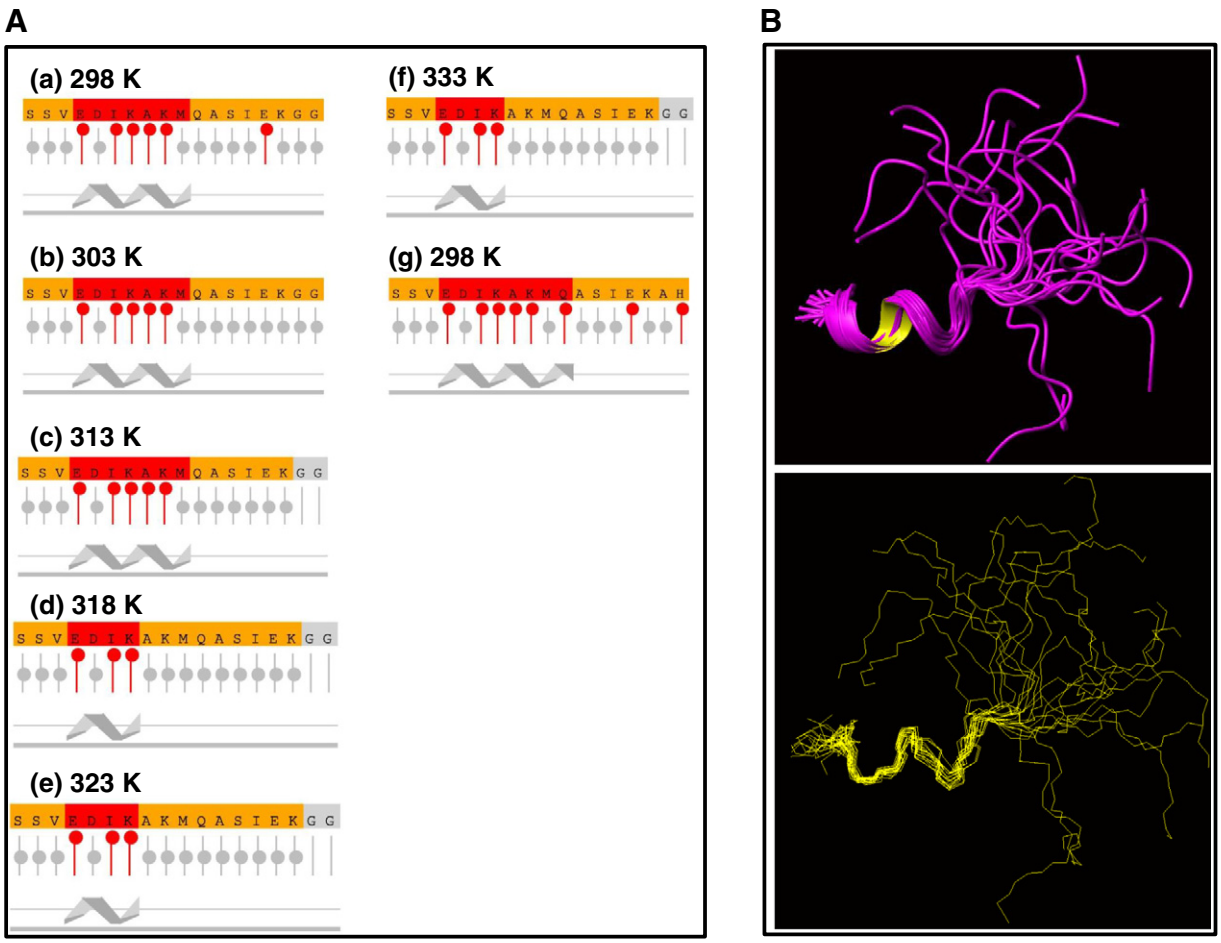

Fig. 5. Correlation between NMR chemical shifts and secondary structure content. Panel A) Hα chemical shift deviations from random coil values (CSD) for NPM1 242–259 B23.1 at (a) 298, (b) 303, (c) 313, (e) 318, (e) 323 and (f) 333 K. (g) Hα chemical shift deviations for NPM1 242–259 B23.2 at 298 K. Graphs were generated with the software NmrView [45] by using as reference random coil chemical shift values proposed by Wishart et al. [47]. In each panel red circles indicate residues with CSD values characteristic of helical secondary structure elements, whereas gray circles represent intermediate deviations equal or close to zero indicative of a residue in a random coil configuration. Peptide regions predicted to be helical are highlighted by the ribbon drawing on the bottom of each panel and corresponding residues are colored red on the amino acid sequence reported on the top. For the NPM1 242–259 B23.1 peptide the last two C-terminal glycines were excluded from the chemical shift analysis in the temperature range 313–333 K, as represented by a line lacking a circle in panels from (c) to (f), due to signal overlaps caused by the increase in temperature. NMR solution structure of NPM1 242–259 B23.1 peptide, Panel B): Superposition on the backbone atoms (residues 242–252) of twenty NPM1 242–259 B23.1 structures (RMSD: 0.96 Å). The ribbon and line representations are shown in the upper and lower panels respectively. The final structure calculation included 74 distance constraints: 30 intra-residues, 28 short- and 16 medium-range and 83 angle constraints. The software MOLMOL [49] has been implemented to generate the figure.

conformation (Fig. 6B). Proton Hα chemical shift changes were monitored as a function of the temperature (298–333 K) and chemical shift deviations from random coil values were estimated to indicate possible changes in the overall helical content. NMR signals that are mainly influenced by temperature are those belonging to H_N protons that become progressively broad and totally disappear at 333 K (Fig. 6B), minor changes are evident and affect the side chain aliphatic protons as well (Fig. A4a, b).

The broadening of H_N lines (Fig. 6B) indicates that by raising the temperature, H_N amide protons become gradually more exposed to the solvent, possibly because a partial unfolding of the pseudo-helical structure takes place. In details, for 242–259 when increasing the temperature the helical content drops from 38.9% to 22.2% (according to CD results) and a residual helical structure is likely to persist between Glu245 and Lys248, as estimated from chemical shift deviations of Hα protons from random coil values (Fig. 5f).

The analysis of the chemical stability of 242–259 was checked by using urea as chaotropic reagent. As shown in Fig. 6C–D, the intensity of the CD signal measured at 222 nm was significantly affected by the addition of even low amounts of the denaturant. Nevertheless, the analysis of the progression of the decrease of the CD signal intensity shows that a significant degree of secondary structure is retained even upon the addition of urea, 8 M. Similar trends were observed for the urea-induced chemical denaturation of 242–259_B23.2 (data not shown).

3.2.3. Fragments of B23.1 and B23.2 C-terminal region are individually able to bind the c-MYC G-quadruplex

The ability of C_107 NPM1-based peptides to bind G-quadruplex was checked by using SPR direct binding assays. These experiments were carried out in the same way of those involving the C_107 NPM1 by using biotinylated c-MYC G-quadruplex as a ligand and the peptides as analytes.

All the C_107 NPM1 regions showed detectable binding to c-MYC G-quadruplex (Table 1). The overlay of the sensorgrams corresponding to the peptide NPM1 188–225 (Fig. 7A–B) showed a clear dose–response binding, in the concentration range of 5–450 μM, and the estimation of K_D value was 18 ± 5 μM, while the affinity of NPM1 225–243 was three-fold lower, since experiments performed in a larger concentration range (10–1000 μM) provided a K_D value of 54 ± 15 μM (Fig. 7C–D). The sequence corresponding to H1 was analyzed in a similar concentration range (50–1200 μM) and data fitting provided a further fifteen-fold higher K_D value of 275 ± 43 μM (Fig. 7E–F). Other variants of NPM1

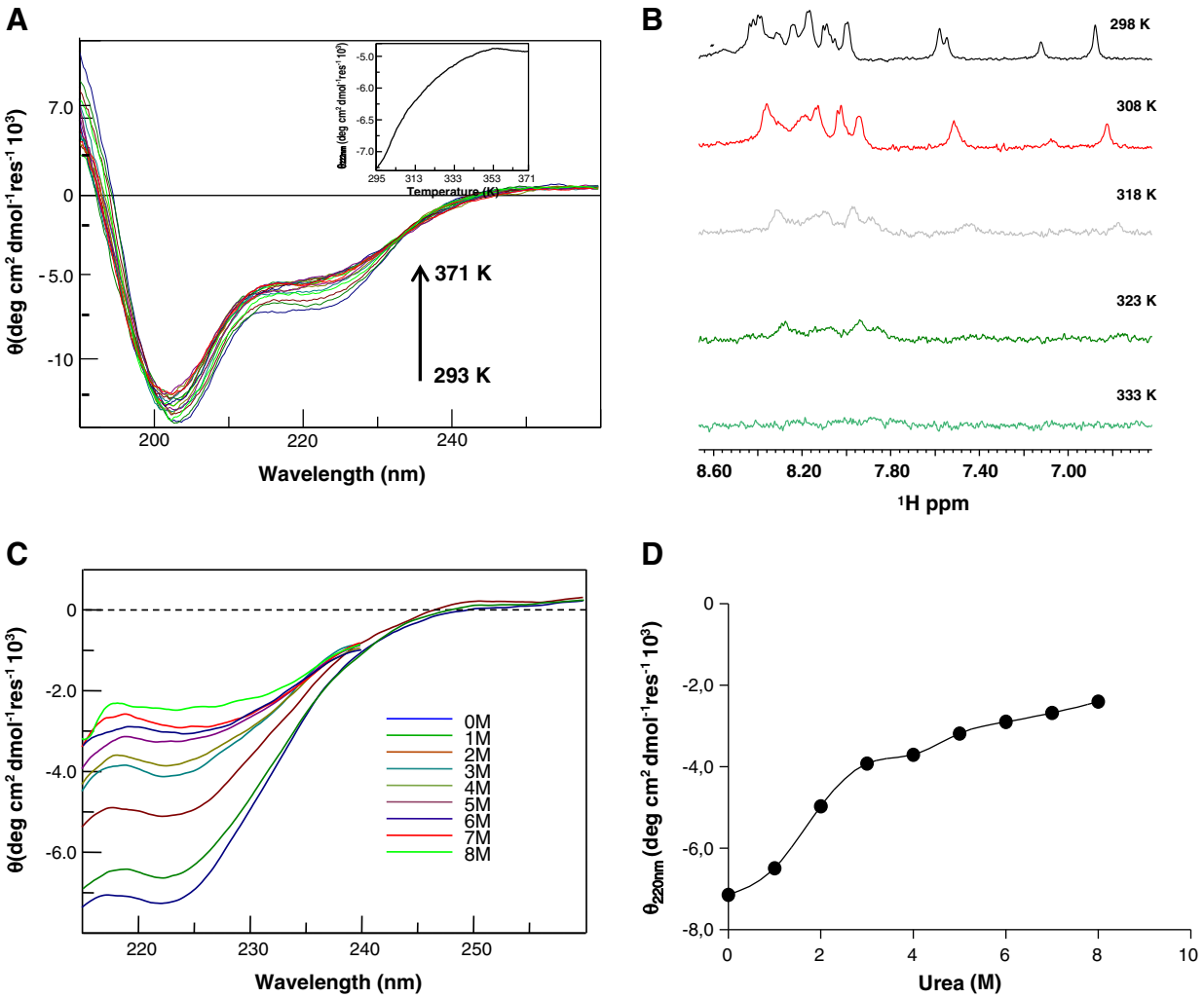

Fig. 6. Analysis of the stability of NPM1 242–259 B23.1 peptide. Overlay of CD spectra registered at (A) different temperatures in the range 293–371 K, as inset of the dependence of ellipticity at 222 nm versus temperature, (C) increasing urea concentrations in the range 0–8 M. In the latter experiment CD spectra were registered in the range 215–260 nm since at lower wavelengths the presence of urea causes too high signal-to-noise ratio; (B) 1D [^{1}H] spectra of NPM1 242–259 B23.1 recorded at different temperatures. In detail, in the reported expansion – from 6.80 to 8.60 ppm – signals arising from backbone and side chain H_N protons can be observed in (D) interpolation of experimental ellipticity at 222 nm versus urea concentration.

242–259 exhibited similar values of K_D toward c-MYC G-quadruplex (Fig. A5). The presence of different residues in the C-terminal region did not substantially affect the binding capacities of H1 variants.

4. Discussion

The involvement of NPM1/B23 in a variety of distinct biological processes is a direct consequence of its ability to establish intermolecular partnerships. The promiscuity of the protein is favored by its modular structure, in which structured domains alternate with disordered regions. Despite the importance of the NPM1/B23 interactions in physiological and pathological conditions, their biophysical and structural characterization is still incomplete. Very recently, it has been shown that the binding of G-quadruplex DNA by NPM1/B23 is important for the nucleolar localization of the protein [52]. The inability of leukemic NPM1/B23 variant to establish this interaction leads to the aberrant cytoplasmic localization of the protein.

Present findings demonstrate that the C-terminal region of the protein is able to bind the c-MYC G-quadruplex with a sub-micromolar affinity. The comparison of these results with previous literature data indicates that the progressive inclusion of portions of the basic region increases the binding affinity of NPM1/B23 for the G-quadruplex sequence. Intriguingly, the inclusion of these regions had also stabilizing effects on the thermal and chemical stabilities of the terminal three helix bundle motif [21,24].

The dissection of NPM1/B23 demonstrates that several fragments of the protein are intrinsically able to bind the G-quadruplex with high affinity. Present data also indicate that, in addition to the unfolded region 225–242, another intrinsically disordered fragment of the protein (residues 188–225) significantly contributes to the binding of the G-quadruplex. Therefore, the tight binding of NPM1/B23 to the G-quadruplex is achieved through the cooperation of both folded and unfolded regions that are individually able to bind it. As mentioned in the Introduction, in the NMR structure of the complex between NPM1 C_70 and the c-MYC G-quadruplex direct interactions with the DNA were established only by the three helix bundle motif [34]. Indeed, the region 225–242 remains flexible without forming any permanent contact with the G-quadruplex. On the other hand, here we show that both regions 188–225 and 225–243 of NPM1/B23 are indeed able to directly bind the G-quadruplex. These apparently contrasting results may be reconciled by assuming that the three helix bundle motif and the disordered basic regions recognize the same regions of the G-quadruplex. In this scenario, the intrinsically disordered regions may play a dual role in the G-quadruplex binding. Taking advantage of the great flexibility, they could efficiently anchor the DNA in the initial stage of the recognition process. Subsequently, after the binding of the G-quadruplex to

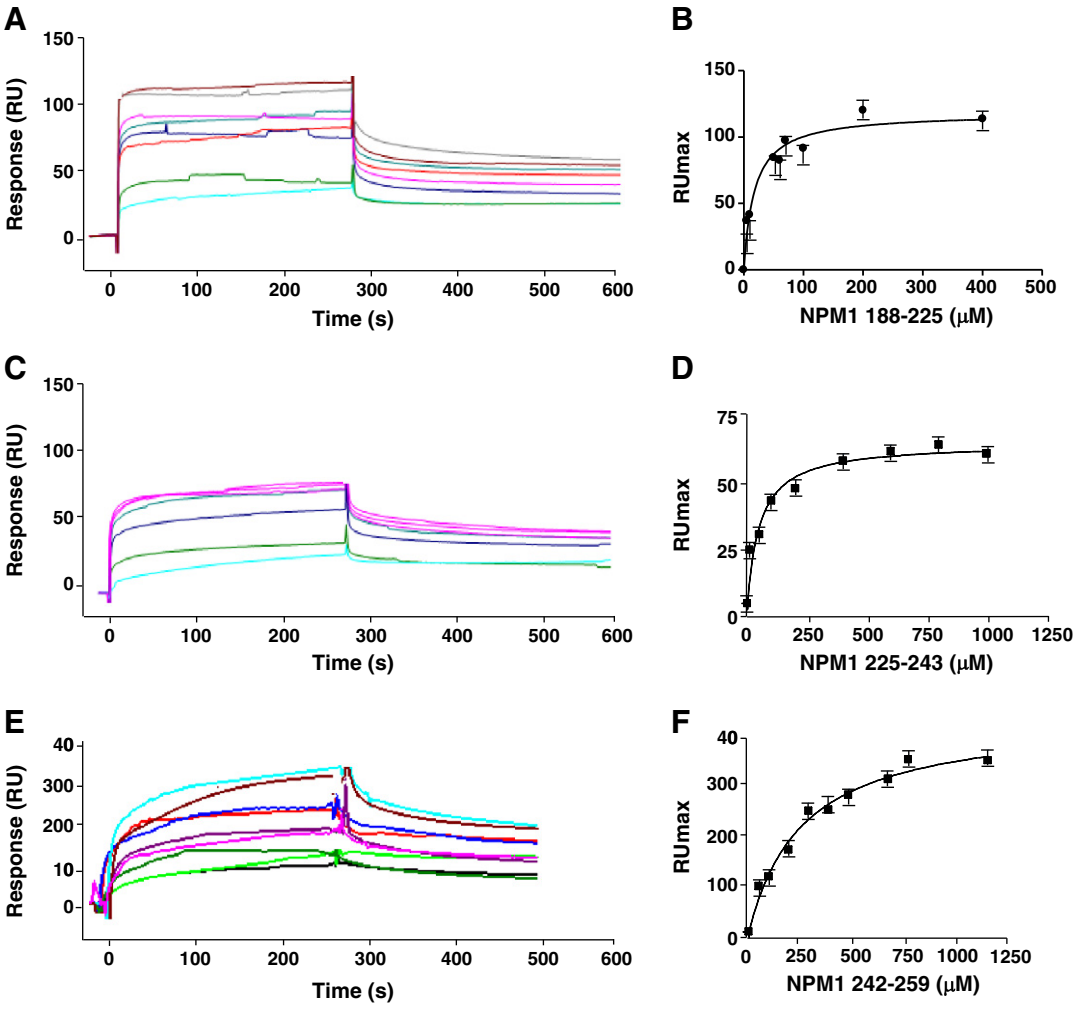

Fig. 7. Binding of C_107NPM1 derived peptides to c-MYC G-quadruplex through SPR. Overlay of sensorgrams for the interaction between biotinylated at 5′ c-MYC G-quadruplex sequence immobilized on a SA (streptavidin) sensor chip and C_107 NPM1 derived peptides. NPM1 (A) 188–225 (C) 225–243, and (E) 242–259 experimental curves that represent different concentrations of analyte and were fitted according to a single exponential binding model with 1:1 stoichiometry, (B), (D), and (F), respectively.

the three helix binding motif, the positively charges of these basic regions may generate a long-range favorable electrostatic environment, as previously suggested [34]. The ability of analyzed peptides to bind c-MYC G-quadruplex represents a solid ground for designing new molecules able to interact with this DNA motif.

The present findings also suggest a reduced G-quadruplex affinity for the two splicing variants B23.2 and B23.3. In particular, a reduced affinity of B23.3 is likely due to the lack of the basic region 195–223 in this isoform. Moreover, the truncation of the C-terminus of the three helix bundle motif to the helix H1 in B23.2 is also expected to strongly decrease the affinity for the G-quadruplex, since we show here that this helix exhibits a significantly reduced affinity, when compared to the whole domain. These suggestions are in line with the results independently obtained by Okuwaki and coworkers, who very recently analyzed the binding of the different NPM1/B23 isoforms and truncated forms to RNA [53]. However, very recently, it has been demonstrated, through ITC analysis, that the affinity of the full-length NPM1 for the same G-quadruplex is 3.8 μM [54] that is a value closer to that one obtained for the C_70 NPM1 than that for the C_107 NPM1. In the case of full-length NPM1 the electrostatic interactions established between the basic domain and the preceding acidic unstructured domains could influence G-quadruplex recognition.

The dissection of NPM1/B23 and the biophysical characterization of the resulting fragments also unveil that the H1 helix of both B23.1 and B23.2 is intrinsically endowed with an unusual thermal stability. A combined CD and NMR analyses show that the N-terminal region of H1 assumes a helical conformation, despite the intrinsic flexibility of the peptides. Indeed, the NMR analysis shows that the segment from Glu245 to Met251 clearly exhibits a tendency to adopt an ordered helical structure. CD and NMR data both indicate that this short helical segment is rather stable upon temperature increase. Evidence of this structure is detected in the entire temperature range (293–371 K for CD and 298–333 K for NMR) explored by using the two techniques. This thermal stability is very unusual for a short peptide that has been derived from a protein sequence. Similar high stabilities have rather been reported, only in few cases, for peptides whose sequences have been ad-hoc designed [51,55]. These unexpected results hold interesting implications for NPM1/B23 folding/unfolding process. In the last years, the folding pathway of several constructs of the NPM1 C-terminal region has been characterized in detail [21–24]. These studies have highlighted the presence of residual structure in the denatured state of the protein [56]. In particular, biophysical characterizations have detected a “native-like” structure that is retained in the denatured state of the wild-type protein, involving the helices H2–H3 of the three helix bundle motif. It has been shown that the presence of these native-like features in the NPM1/B23 denatured state accelerates the folding process. Moreover, it has been suggested that the identification and the characterization of these native-like features may be a way to design new molecules that could restore the native fold in pathological mutants. The intrinsic stability of the H1 helix provides support to the

view that the denatured state retains some native-like structural properties, although in previous analyses this helix was considered to be unfolded. Of particular interest, in this context, is the observation that Trp290 interacts in the native fold with the intrinsically folded N-terminal region of H1. In line with the previous suggestions, this observation may be exploited in future studies for designing molecules able to stabilize the fold of the domain and to restore the protein function in NPM1/B23 mutants.

5. Conclusions

In conclusion this study unveils structural and functional determinants of the interaction between G-quadruplex DNA and NPM1, by analyzing the contribution of single protein regions in DNA recognition mechanism. Through a rational fragmentation approach results clearly indicate a crucial and direct role exerted by IDRs in DNA recognition, speculating a synergic action of IDRs along with H1 region in formation of the complex with G-quadruplex in which the flexible basic fragments primarily allow to accommodate DNA structures. This study shed new light for the design of small molecules and/or peptides able to stabilize G-quadruplex/NPM1complex which could help the research in the field of AML disease.

Acknowledgements

This work was funded in part by the MIUR Ricerca e Competitività 2007–2013 #PON 01_2388. This work was supported by a grant from the Italian Association for Cancer Research (IG14038) to G.T. The authors are grateful to Luca De Luca, Leopoldo Zona and Dr Giuseppe Perretta for the technical assistance, and Prof A. Zagari and Dr V. Granata of CEINGE — NAPOLI for their helpful discussion on SPR experiments.

Appendix A. Supplementary data

Supplementary data to this article can be found online at http://dx.doi.org/10.1016/j.bbagen.2014.02.017.

References

[1] Y.J. Kang, M.O. Olson, C. Jones, H. Busch, Nucleolar phosphoproteins of normal rat liver and Novikoff hepatoma ascites cells, Cancer Res. 35 (1975) 1470–1475.
[2] M. Okuwaki, K. Matsumoto, M. Tsujimoto, K. Nagata, Function of nucleophosmin/B23, a nucleolar acidic protein, as a histone chaperone, FEBS Lett. 506 (2001) 272–276.
[3] R.A. Borer, C.F. Lehner, H.M. Eppenberger, E.A. Nigg, Major nucleolar proteins shuttle between nucleus and cytoplasm, Cell 56 (1989) 379–390.
[4] M. Okuwaki, A. Iwamatsu, M. Tsujimoto, K. Nagata, Identification of nucleophosmin/B23, an acidic nucleolar protein, as a stimulatory factor for in vitro replication of adenovirus DNA complexed with viral basic core proteins, J. Mol. Biol. 311 (2001) 41–55.
[5] M.S. Lindstrom, NPM1/B23: a multifunctional chaperone in ribosome biogenesis and chromatin remodeling, Biochem. Res. Int. (2011) 195209 (16 pp.).
[6] L.B. Maggi Jr., M. Kuchenruether, D.Y. Dadey, R.M. Schwope, S. Grisendi, R.R. Townsend, P.P. Pandolfi, J.D. Weber, Nucleophosmin serves as a rate-limiting nuclear export chaperone for the mammalian ribosome, Mol. Cell. Biol. 28 (2008) 7050–7065.
[7] E. Colombo, M. Alcalay, P.G. Pelicci, Nucleophosmin and its complex network: a possible therapeutic target in hematological diseases, Oncogene 30 (2011) 2595–2609.
[8] J.P. Yun, J. Miao, G.G. Chen, Q.H. Tian, C.Q. Zhang, J. Xiang, J. Fu, P.B. Lai, Increased expression of nucleophosmin/B23 in hepatocellular carcinoma and correlation with clinicopathological parameters, Br. J. Cancer 96 (2007) 477–484.
[9] S. Grisendi, C. Mecucci, B. Falini, P.P. Pandolfi, Nucleophosmin and cancer, Nat. Rev. Cancer 6 (2006) 493–505.
[10] R. Balusu, W. Fiskus, R. Rao, D.G. Chong, S. Nalluri, U. Mudunuru, H. Ma, L. Chen, S. Venkannagari, K. Ha, S. Abhyankar, C. Williams, J. McGuirk, H.J. Khoury, C. Ustun, K.N. Bhalla, Targeting levels or oligomerization of nucleophosmin 1 induces differentiation and loss of survival of human AML cells with mutant NPM1, Blood 118 (2011) 3096–3106.
[11] B. Falini, I. Nicoletti, N. Bolli, M.P. Martelli, A. Liso, P. Gorello, F. Mandelli, C. Mecucci, M.F. Martelli, Translocations and mutations involving the nucleophosmin (NPM1) gene in lymphomas and leukemias, Haematologica 92 (2007) 519–532.
[12] B. Falini, C. Mecucci, E. Tiacci, M. Alcalay, R. Rosati, L. Pasqualucci, R. La Starza, D. Diverio, E. Colombo, A. Santucci, B. Bigerna, R. Pacini, A. Pucciarini, A. Liso, M. Vignetti, P. Fazi, N. Meani, V. Pettirossi, G. Saglio, F. Mandelli, F. Lo-Coco, P.G. Pelicci, M.F. Martelli, Cytoplasmic nucleophosmin in acute myelogenous leukemia with a normal karyotype, N. Engl. J. Med. 352 (2005) 254–266.
[13] B. Falini, N. Bolli, J. Shan, M.P. Martelli, A. Liso, A. Pucciarini, B. Bigerna, L. Pasqualucci, R. Mannucci, R. Rosati, P. Gorello, D. Diverio, G. Roti, E. Tiacci, G. Cazzaniga, A. Biondi, S. Schnittger, T. Haferlach, W. Hiddemann, M.F. Martelli, W. Gu, C. Mecucci, I. Nicoletti, Both carboxy-terminus NES motif and mutated tryptophan(s) are crucial for aberrant nuclear export of nucleophosmin leukemic mutants in NPMc + AML, Blood 107 (2006) 4514–4523.
[14] B. Falini, I. Nicoletti, M.F. Martelli, C. Mecucci, Acute myeloid leukemia carrying cytoplasmic/mutated nucleophosmin (NPMc + AML): biologic and clinical features, Blood 109 (2007) 874–885.
[15] M. Okuwaki, A. Sumi, M. Hisaoka, A. Saotome-Nakamura, S. Akashi, Y. Nishimura, K. Nagata, Function of homo- and hetero-oligomers of human nucleoplasmin/nucleophosmin family proteins NPM1, NPM2 and NPM3 during sperm chromatin remodeling, Nucleic Acids Res. 40 (2012) 4861–4878.
[16] M. Okuwaki, The structure and functions of NPM1/nucleophosmin/B23, a multifunctional nucleolar acidic protein, J. Biochem. 143 (2008) 441–448.
[17] V.M. Namboodiri, I.V. Akey, M.S. Schmidt-Zachmann, J.F. Head, C.W. Akey, The structure and function of *Xenopus* NO38-core, a histone chaperone in the nucleolus, Structure 12 (2004) 2149–2160.
[18] H.H. Lee, H.S. Kim, J.Y. Kang, B.I. Lee, J.Y. Ha, H.J. Yoon, S.O. Lim, G. Jung, S.W. Suh, Crystal structure of human nucleophosmin-core reveals plasticity of the pentamer–pentamer interface, Proteins 69 (2007) 672–678.
[19] C.G. Grummitt, F.M. Townsley, C.M. Johnson, A.J. Warren, M. Bycroft, Structural consequences of nucleophosmin mutations in acute myeloid leukemia, J. Biol. Chem. 283 (2008) 23326–23332.
[20] L. Federici, B. Falini, Nucleophosmin mutations in acute myeloid leukemia: a tale of protein unfolding and mislocalization, Protein Sci. 22 (2013) 545–556.
[21] D. Marasco, A. Ruggiero, C. Vascotto, M. Poletto, P.L. Scognamiglio, G. Tell, L. Vitagliano, Role of mutual interactions in the chemical and thermal stability of nucleophosmin NPM1 domains, Biochem. Biophys. Res. Commun. 430 (2013) 523–528.
[22] F. Scaloni, L. Federici, M. Brunori, S. Gianni, Deciphering the folding transition state structure and denatured state properties of nucleophosmin C-terminal domain, Proc. Natl. Acad. Sci. U. S. A. 107 (2010) 5447–5452.
[23] F. Scaloni, S. Gianni, L. Federici, B. Falini, M. Brunori, Folding mechanism of the C-terminal domain of nucleophosmin: residual structure in the denatured state and its pathophysiological significance, FASEB J. 23 (2009) 2360–2365.
[24] S. Chiarella, L. Federici, A. Di Matteo, M. Brunori, S. Gianni, The folding pathway of a functionally competent C-terminal domain of nucleophosmin: protein stability and denatured state residual structure, Biochem. Biophys. Res. Commun. 435 (2013) 64–68.
[25] D. Fantini, C. Vascotto, D. Marasco, C. D'Ambrosio, M. Romanello, L. Vitagliano, C. Pedone, M. Poletto, L. Cesaratto, F. Quadrifoglio, A. Scaloni, J.P. Radicella, G. Tell, Critical lysine residues within the overlooked N-terminal domain of human APE1 regulate its biological functions, Nucleic Acids Res. 38 (2010) 8239–8256.
[26] M. Hisaoka, S. Ueshima, K. Murano, K. Nagata, M. Okuwaki, Regulation of nucleolar chromatin by B23/nucleophosmin jointly depends upon its RNA binding activity and transcription factor UBF, Mol. Cell. Biol. 30 (2010) 4952–4964.
[27] E. Colombo, J.C. Marine, D. Danovi, B. Falini, P.G. Pelicci, Nucleophosmin regulates the stability and transcriptional activity of p53, Nat. Cell Biol. 4 (2002) 529–533.
[28] C. Lee, B.A. Smith, K. Bandyopadhyay, R.A. Gjerset, DNA damage disrupts the p14ARF-B23(nucleophosmin) interaction and triggers a transient subnuclear redistribution of p14ARF, Cancer Res. 65 (2005) 9834–9842.
[29] Y. Jian, Z. Gao, J. Sun, Q. Shen, F. Feng, Y. Jing, C. Yang, RNA aptamers interfering with nucleophosmin oligomerization induce apoptosis of cancer cells, Oncogene 28 (2009) 4201–4211.
[30] S.S. Gadad, R.E. Rajan, P. Senapati, S. Chatterjee, J. Shandilya, P.K. Dash, U. Ranga, T.K. Kundu, HIV-1 infection induces acetylation of NPM1 that facilitates Tat localization and enhances viral transactivation, J. Mol. Biol. 410 (2011) 997–1007.
[31] D. Wang, A. Baumann, A. Szebeni, M.O. Olson, The nucleic acid binding activity of nucleolar protein B23.1 resides in its carboxyl-terminal end, J. Biol. Chem. 269 (1994) 30994–30998.
[32] T.S. Dumbar, G.A. Gentry, M.O. Olson, Interaction of nucleolar phosphoprotein B23 with nucleic acids, Biochemistry 28 (1989) 9495–9501.
[33] L. Federici, A. Arcovito, G.L. Scaglione, F. Scaloni, C. Lo Sterzo, A. Di Matteo, B. Falini, B. Giardina, M. Brunori, Nucleophosmin C-terminal leukemia-associated domain interacts with G-rich quadruplex forming DNA, J. Biol. Chem. 285 (2010) 37138–37149.
[34] A. Gallo, C. Lo Sterzo, M. Mori, A. Di Matteo, I. Bertini, L. Banci, M. Brunori, L. Federici, Structure of nucleophosmin DNA-binding domain and analysis of its complex with a G-quadruplex sequence from the c-MYC promoter, J. Biol. Chem. 287 (2012) 26539–26548.
[35] S. Burge, G.N. Parkinson, P. Hazel, A.K. Todd, S. Neidle, Quadruplex DNA: sequence, topology and structure, Nucleic Acids Res. 34 (2006) 5402–5415.
[36] A. Siddiqui-Jain, C.L. Grand, D.J. Bearss, L.H. Hurley, Direct evidence for a G-quadruplex in a promoter region and its targeting with a small molecule to repress c-MYC transcription, Proc. Natl. Acad. Sci. U. S. A. 99 (2002) 11593–11598.
[37] C. Vascotto, D. Fantini, M. Romanello, L. Cesaratto, M. Deganuto, A. Leonardi, J.P. Radicella, M.R. Kelley, C. D'Ambrosio, A. Scaloni, F. Quadrifoglio, G. Tell, APE1/Ref-1 interacts with NPM1 within nucleoli and plays a role in the rRNA quality control process, Mol. Cell. Biol. 29 (2009) 1834–1854.
[38] M. Poletto, C. Vascotto, P.L. Scognamiglio, L. Lirussi, D. Marasco, G. Tell, Role of the unstructured N-terminal domain of the hAPE1 (human apurinic/apyrimidinic endonuclease 1), Biochem. J. 452 (2013) 545–557.
[39] R.L. Rich, D.G. Myszka, Advances in surface Plasmon resonance biosensor analysis, Curr. Opin. Biotechnol. 11 (2000) 54–61.
[40] G.B. Fields, R.L. Noble, Solid phase peptide synthesis utilizing 9-fluorenylmethoxycarbonyl amino acids, Int. J. Pept. Protein Res. 35 (1990) 161–214.

[41] C. Griesinger, G. Otting, K. Wuthrich, R.R. Ernst, Clean TOCSY for H-1 spin system-identification in macromolecules, J. Am. Chem. Soc. 110 (1988) 7870–7872.
[42] A. Kumar, R.R. Ernst, K. Wuthrich, A two-dimensional nuclear overhauser enhancement (2D NOE) experiment for the elucidation of complete proton–proton cross-relaxation networks in biological macromolecules, Biochem. Biophys. Res. Commun. 95 (1980) 1–6.
[43] C. Dalvit, Efficient multiple-solvent suppression for the study of the interactions of organic solvents with biomolecules, J. Biomol. NMR 11 (1998) 437–444.
[44] C. Bartels, T.H. Xia, M. Billeter, P. Guntert, K. Wuthrich, The program XEASY for computer-supported NMR spectral analysis of biological macromolecules, J. Biomol. NMR 6 (1995) 1–10.
[45] B.A. Johnson, Using NMRView to visualize and analyze the NMR spectra of macromolecules, Methods Mol. Biol. 278 (2004) 313–352.
[46] S. Schwarzinger, G.J. Kroon, T.R. Foss, P.E. Wright, H.J. Dyson, Random coil chemical shifts in acidic 8 M urea: implementation of random coil shift data in NMRView, J. Biomol. NMR 18 (2000) 43–48.
[47] D.S. Wishart, C.G. Bigam, A. Holm, R.S. Hodges, B.D. Sykes, 1H, 13C and 15N random coil NMR chemical shifts of the common amino acids. I. Investigations of nearest-neighbor effects, J. Biomol. NMR 5 (1995) 67–81.
[48] T. Herrmann, P. Guntert, K. Wuthrich, Protein NMR structure determination with automated NOE assignment using the new software CANDID and the torsion angle dynamics algorithm DYANA, J. Mol. Biol. 319 (2002) 209–227.
[49] R. Koradi, M. Billeter, K. Wuthrich, MOLMOL: a program for display and analysis of macromolecular structures, J. Mol. Graph. 14 (1996) 51–55 (29–32).
[50] K. Wüthrich, NMR of Proteins and Nucleic Acids, John Wiley & Sons, New York, 1986.
[51] N.E. Shepherd, H.N. Hoang, G. Abbenante, D.P. Fairlie, Single turn peptide alpha helices with exceptional stability in water, J. Am. Chem. Soc. 127 (2005) 2974–2983.
[52] S. Chiarella, A. De Cola, G.L. Scaglione, E. Carletti, V. Graziano, D. Barcaroli, C. Lo Sterzo, A. Di Matteo, C. Di Ilio, B. Falini, A. Arcovito, V. De Laurenzi, L. Federici, Nucleophosmin mutations alter its nucleolar localization by impairing G-quadruplex binding at ribosomal DNA, Nucleic Acids Res. 41 (2013) 3228–3239.
[53] M. Hisaoka, K. Nagata, M. Okuwaki, Intrinsically disordered regions of nucleophosmin/B23 regulate its RNA binding activity through their inter- and intra-molecular association, Nucleic Acids Res. 17 (2014) 1180–1195.
[54] S. Banuelos, B. Lectez, S.G. Taneva, G. Ormaza, M. Alonso-Marino, X. Calle, M.A. Urbaneja, Recognition of intermolecular G-quadruplexes by full length nucleophosmin. Effect of a leukaemia-associated mutation, FEBS Lett. 587 (2013) 2254–2259.
[55] D. Diana, B. Ziaco, G. Colombo, G. Scarabelli, A. Romanelli, C. Pedone, R. Fattorusso, L.D. D'Andrea, Structural determinants of the unusual helix stability of a de novo engineered vascular endothelial growth factor (VEGF) mimicking peptide, Chemistry 14 (2008) 4164–4166.
[56] I.E. Sanchez, T. Kiefhaber, Hammond behavior versus ground state effects in protein folding: evidence for narrow free energy barriers and residual structure in unfolded states, J. Mol. Biol. 327 (2003) 867–884.